Measurement of Satellite Solar Array Panel Vibrations Caused by Thermal Snap and Gas Jet Thruster Firing

Mitsushige Oda[1], Yusuke Hagiwara[2], Satoshi Suzuki[3],
Toshiyuki Nakamura[1], Noriyasu Inaba[1], Hirotaka Sawada[1],
Masahiro Yoshii[1] and Naoki Goto[1]

[1]Japan Aerospace Exploration Agency (JAXA)
[2]Tokyo Institute of Technology
[3]AES Co., Ltd
Japan

1. Introduction

Many space satellites have large solar array paddles (Fig. 1) for power generation and large antennas for observation and communication. These large space structures are folded during transport into space by launch vehicles, and deployed after arriving in space. The paddles and antennas must be lightweight because of the payload weight limit of the launch vehicle and are therefore very flexible, with little damping ability. This results in vibrations, which cause serious problems. In particular, there have been increasing demands for enhanced resolution of Earth observations from low Earth orbiting satellites in recent years. Accordingly, the requirements for satellite attitude stability are also increasing. Conversely, it is also known that the attitude stability of low Earth orbiting satellites is disturbed when the satellites go into and leave an eclipse. When the thermal environment around a flexible structure on orbit such as a solar array paddle changes to cold or hot, the flexible structure
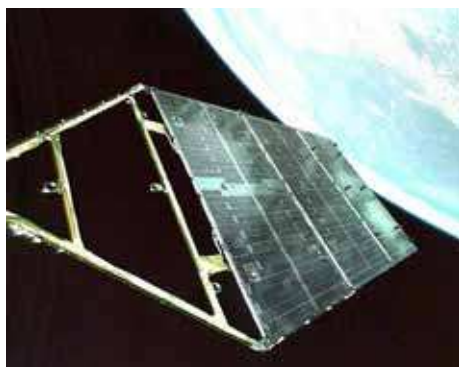

Fig. 1. A solar array paddle in orbit © JAXA

produces its own deformation or vibration. These occur most often during rapid temperature changes called thermal snap or thermally-induced vibration, which has been known to cause attitude disturbance in Low Earth Orbit (LEO) satellites.

Thermal snap vibration occurring on a flexible solar array panel is very slow, and measuring motion on a solar array panel caused by thermal snap with sensors, such as an accelerometer, is very difficult. The behaviour of a space structure affected by thermal snap has never been observed directly in space until now. In this chapter, our vibration measurement method, along with images taken in space and the image processing conducted with the images taken on the ground, is explained, and some measurement results are shown.

2. Thermal snap

Thermal snap is a unique phenomenon affecting flexible space structures and one of the main factors causing disturbances in satellites. When a satellite enters an eclipse, the whole of the solar array paddle or solar array panels are subject to rapid cooling, while the temperature of the panel on the sun side is high beforehand. When the satellite leaves the eclipse, the sun side of the solar array panels heats up rapidly, while the temperature difference between both sides of the solar array panel is small when the satellite is in the eclipse.

These rapid changes of temperature difference between both sides of the solar array panels result in thermal expansion and shrinking of the solar array panels and cause the solar array panels to bend. This bending then, in turn, causes the solar array panels to vibrate and results in degradation of the satellite attitude stability.

Many past satellites and space structures observed thermal snap from their attitude data. The Hubble Space Telescope (HST) shown in Fig. 2 was launched by the space shuttle *Discovery* on April 25, 1990, to conduct higher-accuracy astronomical observations than ground-based equipment (Foster et al., 1995). A pointing control system of HST was designed to hold an image stable at the HST focal plane to 0.007 arcsec (rms) for the duration of an observation. However, following successful deployment of a pair of solar array paddles, gyro data revealed significant attitude disturbances; observed when HST entered or left the shadow of the earth. Based on investigation of HST's telemetry data and certain analyses, it was concluded that the disturbance of HST was caused by the thermally-induced deformation of the HST solar array paddle. The HST solar array paddle has a flexible solar array blanket and deploys a boom named the two-element Storable Tubular Extendible Member (Bi-STEM). When HST remains in orbit on the day side, its deploying boom heats up and a thermal gradient appears. The surface directed toward the Sun is hotter than the opposite one and the thermal gradient also causes the solar array paddle to bend. Conversely, when HST is in orbit on the night side, the whole of the boom cools down and the thermal gradient disappears, while the bending of the solar array paddle is also absent. This bending motion occurs rapidly during sunshine/ eclipse transition and disrupts HST's pointing system. In December 1993, the space shuttle *Endeavour* was launched and the solar array paddles were replaced with new units to counter the problem.

The Upper Atmosphere Research Satellite (UARS), launched in September 1991, and the Advanced Land Observing Satellite (ALOS), launched in January 2006, in addition to HST, also observed an attitude disturbance of the main body based on gyro telemetry data when they traversed boundaries between the orbital day and night sides (Iwata et al., 2006; Johnston & Thornton, 2000). However, these phenomena are rarely observed or measured

Fig. 2. Hubble Space Telescope

directly since the solar array panel motions caused by thermal snap are very slow and difficult to measure using sensors such as accelerometers. Additionally, the measurement system has to be compact because of the strict payload limit, meaning there have been hardly any direct measurements of thermal snap in orbit to date.

3. Measurement system using an onboard monitoring camera

This section introduces the equipment and configuration of our measurement system. To measure vibration on flexible space structures, we proposed a method using a single monitoring camera mounted on a satellite, the latter of which has several monitoring cameras to monitor its own states. Our measurement system uses one of them, which monitors solar array paddles.

3.1 GOSAT

Our measurement system is installed on JAXA's (Japan Aerospace Exploration Agency) Earth observation satellite named GOSAT (Greenhouse gases Observing Satellite), and measures the deformation and vibration of its solar array paddle. GOSAT was launched on January 2009. Its major parameters are shown in Table 1, and an overall view in Fig. 3.

Size	Main body	3.7 m (H) × 1.8 m (W) × 2.0 m (D)
	Wingspan	13.7 m
Mass		1750 kg
Power		3.8 kW
Lifespan		5 years
Orbit		Sun Synchronous Orbit
	Local time	13:00 ± 0:15
	Attitude	666 km
	Inclination	98 deg
	Re-visit	3 days
Launch	Vehicle	H-IIA
	Schedule	Jan. 2009

Table 1. GOSAT Summary

S-band Antenna

Technical Data Acquisition Equipment (TEDA)

Monitor Camera(CAM)

TANSO-FTS: Greenhouse Gases Sensor

Solar array panel

Solar array panel

Nadir

TANSO-CAI: Cloud and Aerosol sensor
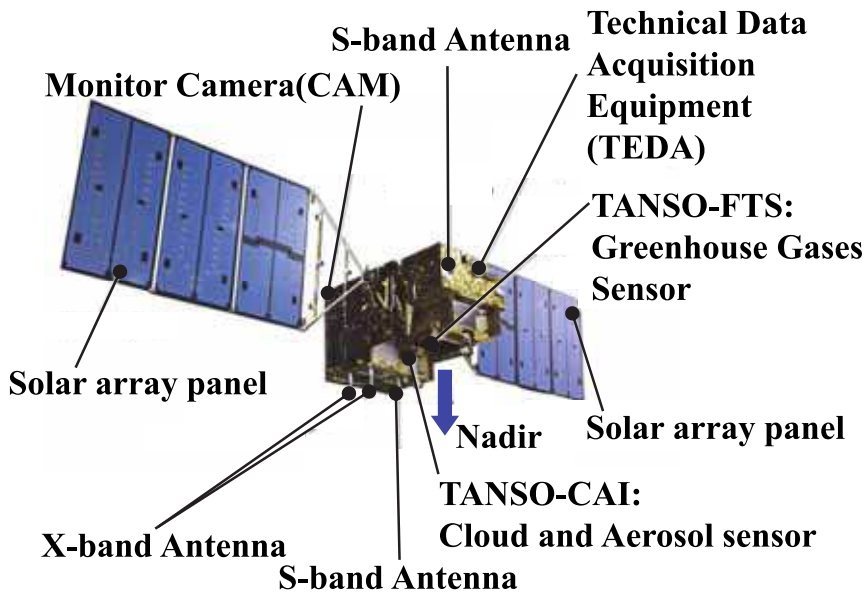
X-band Antenna

S-band Antenna

Fig. 3. Overall view of GOSAT

GOSAT has eight CMOS cameras to monitor the deployment state of solar array paddles, their post-deployment behaviour, the existence of contamination in the opening of fairing, separation of the satellite from a launch vehicle, and so on. The effective sensor resolution of the cameras is 1.3 million pixels. The monitoring camera which we used for monitoring the whole of the solar array paddle thus has a short focal length and a wide view angle while the monitoring camera we used for measurement is shown in Fig. 4 and has an LED lighting system.

Fig. 4. Monitoring camera mounted on GOSAT © Meisei Electric Co., Ltd.

3.2 Assumptions to measure the vibration
The solar array panel's vibration is measured using one CMOS camera mounted on the satellite main body. Since the images taken by a single CMOS camera do not include 3-D information, some assumptions are needed to identify the vibration of the solar array panels. The major assumptions are as follows:

3.2.1 Solar array panel
The GOSAT has a pair of solar array paddles, unlike most remote sensing satellites in low Earth orbits, which have only one. This is to improve robustness against failures in the solar array paddle, which resulted in the total loss of the ADEOS and ADEOS-II, which are JAXA's former remote sensing satellites. Each paddle consists of three semi-rigid panels and a yoke. These solar panels were folded down to the satellite main body during the rocket launch and released in orbit. During this measurement, we consider the solar paddle, which comprises three panels, to be actually a single uniform panel. Fig. 5 shows the size of the solar array paddle and its visual markers, namely about 2800×6000 mm.
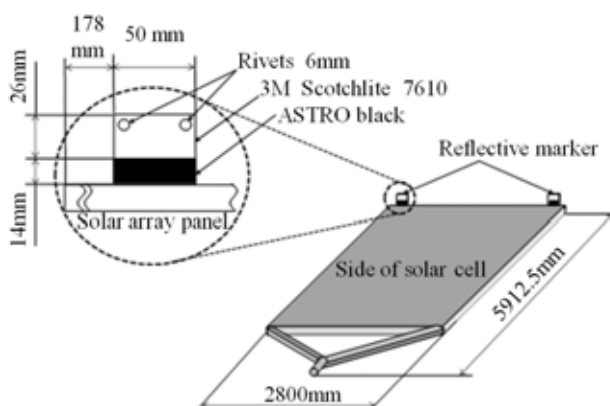

Fig. 5. Size of the solar array paddle and its visual marker

3.2.2 Visual markers
The vibration of the solar array paddle caused by thermal snap occurs during poor lighting conditions for the monitoring camera (eclipse). Additionally, the lighting condition changes dramatically while the satellite goes from sunshine into the eclipse. Visual markers and an LED lighting system are used to help Interference the motion of the solar array paddle. The visual marker is made of reflective tape and is 50×26 mm in size. Unfortunately, these markers are attached only to the front surface (solar cell side) of the solar paddle, to avoid mechanical interface with the solar cell panels when they are folded down to the satellite main body. Displacement of the solar array paddle can be obtained by measuring the positions of the Visual markers.

3.2.3 Vibration modes
We assumed that the GOSAT's solar array paddle has three major vibration modes as shown in Fig. 6, namely out-of-plane vibrations, twists, and in-plane vibrations. Higher order vibrations are not considered.
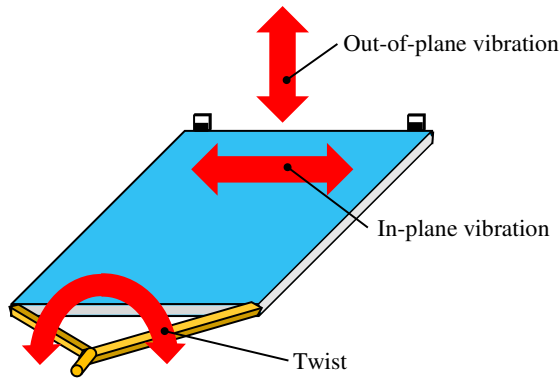
Fig. 6. Vibration modes of the solar array panel

3.3 Ground-based test model for the algorithm development

To develop the measurement system and algorithm, a ground-based test model comprising a scale model (1/ 3 scale) of the solar cell paddle, a compatible CMOS camera and an LED lighting system are developed. An artist's image of the test bed is shown in Fig. 7, and that of the solar array paddle taken by the ground-based test model is shown in Fig. 8.
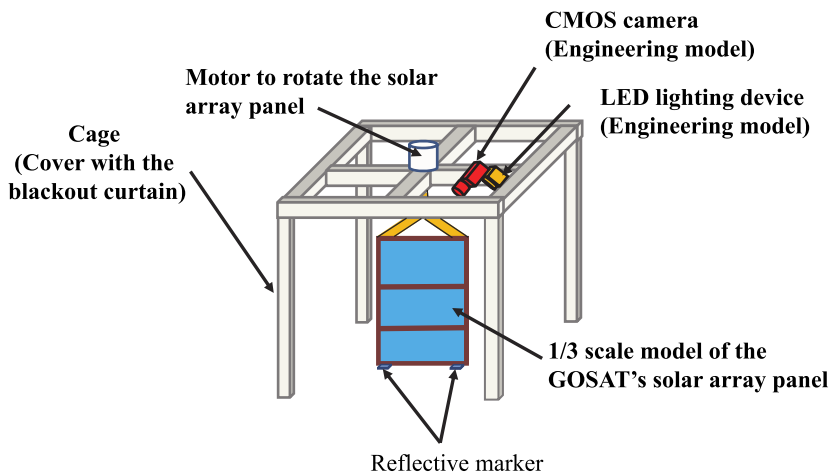
Fig. 7. A ground-based test model to develop the measurement system

4. Development of a high-accuracy image processing algorithm

Images taken by the mounted camera are down-linked to the ground and subject to processing to measure the position of the reflective markers. The algorithm for the image processing is shown in this section. One problem when measuring thermal snap is that the lighting condition changes dramatically during the measurement. To resolve this, the image processing algorithm is adjusted to use the same algorithm for both sunshine and eclipse. A ground-based test model was used to develop our measurement system.
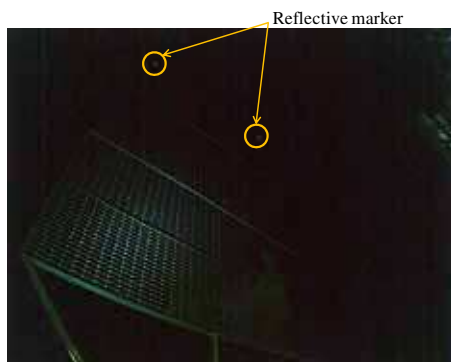
Fig. 8. Image of the solar array paddle taken by the test bed

4.1 Calibration of camera parameters

Since the CMOS camera optical lens system is usually simple, the images taken always include distortion, which must be corrected. Image data processing, such as searching the visual marker, is based on MVTech's HALCON system.

The camera parameters are necessary to obtain the marker position by image processing and include internal and external camera parameters. The internal camera parameter comprises eight items of Focus, Kappa, Sx, Sy, Cx, Cy, Image width and Image height. Focus is the focal length of the lens. Kappa is the distortion coefficient of the lens. Sx and Sy are the distances between the cells. Cx and Cy are coordinates at the distortion centre. The external camera parameter shows the relation between the measurement plane and the camera (position and orientation). This camera parameter can be easily obtained by using the camera calibration program installed in HALCON.

Fig. 9 shows the standard calibration table of HALCON, which is used for its calibration. Since the black spot of the standard calibration table interval is already known, the camera parameter can be obtained by taking a photograph of the standard calibration plate.

Fig. 10 shows the image of the calibration. A standard calibration table is taken of a photograph 20 times while changing the relation of the camera (position and orientation). Afterwards, the standard calibration table is set up in the measurement plane, and a photograph is taken. The internal and external camera parameters were calculated using these 21 images.
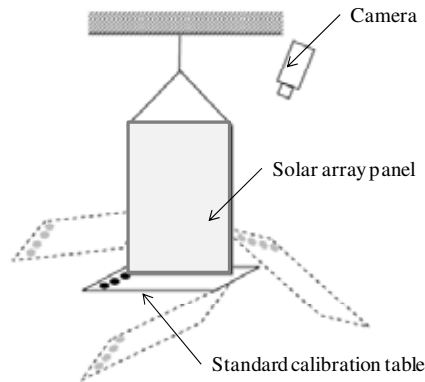

Fig. 9. Calibration table

Fig. 10. Calibration method using a standard calibration table

4.2 Development of the image processing algorithm

Fig. 11 is the flow chart used to obtain the position of the marker from the image. Initially, the image is converted into gray scale, whereupon the marker candidate area is searched for, using the entire image. The edge extraction processing is then performed in the marker candidate area, with the marker and noise distinguished by the length, size, and circularity of the extracted edge. If the number of edges that remove the noise is two, the edges are considered markers. Subsequently, the centre of the marker is obtained in the image coordinate system [Row, Column] (pixel) and converted into a world coordinate system [X, Y] (mm) by the camera parameter. The distance between the two markers is calculated, and the correctness of the value is determined. When the image processing is not the first frame, the distance the marker has moved from the previous frame is calculated. If this numerical result is correct, the image processing is considered a success. When this happens, the surround of the marker position of the present frame is assumed to be a marker candidate area of the following frame.

Fig. 12 is the image processing result. The marker to the left of the screen is called No. 0 and the other marker is called No. 1. This figure shows successful marker extraction through image processing, with Fig. 13 a transition of the distance between the two markers. The accuracy of the image processing can be shown by the size of the change of the distance between the two markers, hence the standard deviation of the distance between markers was assumed to represent the image processing accuracy. In the ground experiment, this value was about 0.99 mm, which corresponds to about 1/5 of the resolution. This result shows that image processing, the accuracy of which exceeds the image resolution, is realized on the ground.

4.3 Adjusting the algorithm for edge extraction

Edge extraction is applied to find markers in our algorithm. One problem when measuring thermal snap, however, is that the lighting condition changes dramatically during the measurement. One kind of algorithm for finding markers should be used under every lighting condition. To resolve this problem, the image processing algorithm is adjusted to use the same algorithm in both sunshine and eclipse. Subsequently, the algorithm is upgraded to enable markers not only when the satellite is in the umbra but also when it is in the sunshine and penumbra, based on the algorithm for the inside of the eclipse. The following are the contents of the upgrade of the algorithm.
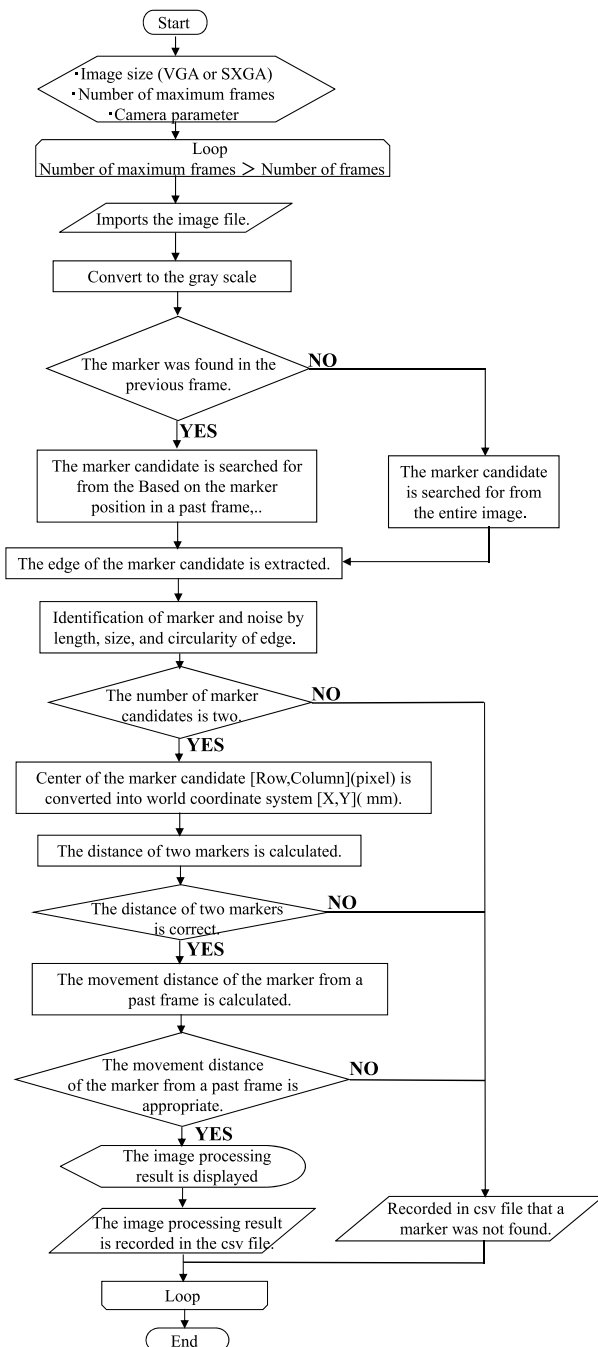
Start

·Image size (VGA or SXGA)
·Number of maximum frames
·Camera parameter

Loop
Number of maximum frames ＞ Number of frames

Imports the image file.

Convert to the gray scale

The marker was found in the previous frame. — NO

YES

The marker candidate is searched for from the Based on the marker position in a past frame,..

The marker candidate is searched for from the entire image.

The edge of the marker candidate is extracted.

Identification of marker and noise by length, size, and circularity of edge.

The number of marker candidates is two. — NO

YES

Center of the marker candidate [Row,Column](pixel) is converted into world coordinate system [X,Y](mm).

The distance of two markers is calculated.

The distance of two markers is correct. — NO

YES

The movement distance of the marker from a past frame is calculated.

The movement distance of the marker from a past frame is appropriate. — NO

YES

The image processing result is displayed

The image processing result is recorded in the csv file.

Recorded in csv file that a marker was not found.

Loop

End

Fig. 11. Algorithm to find the marker in the images
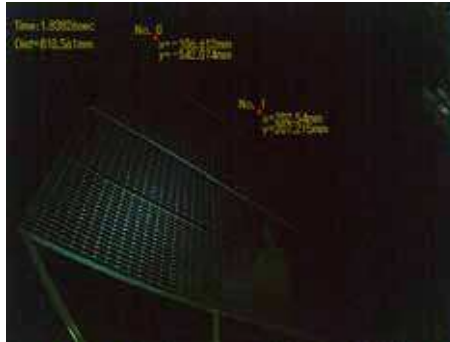
Fig. 12. The image processing result using the ground-based test model
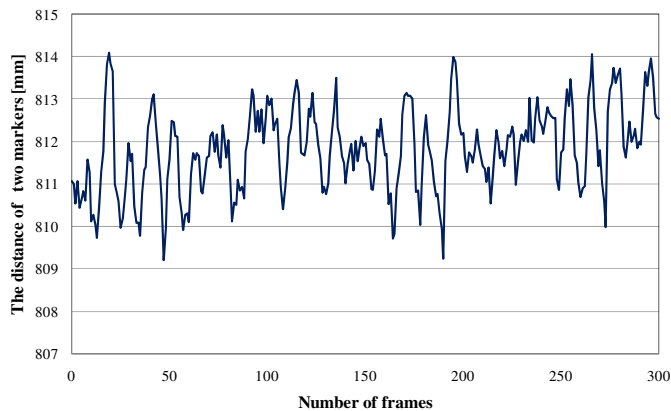
Fig. 13. Transition of the distance between two markers on the ground

4.3.1 Detecting the marker candidate area

Many lighting points have equivalent size and shape when compared to actual markers in the sunshine and penumbra. Therefore, when the analysis starts, the marker candidate area is specified manually in the new algorithm. Subsequently, if the image processing is successful, the marker candidate area in the next frame is specified at near the current marker candidate area.

4.3.2 Determining the threshold for finding markers

The thresholds for finding markers change depending on the luminance of the marker candidate area in the upgraded algorithm, since this changes around the time when the satellite goes into eclipse.

4.3.3 Parameter for distinguishing the marker and noise

The conditions for distinguishing the marker and noise, for example, the size and circularity of the extracted edges, are relaxed. This is because a true marker is often mistakenly distinguished as noise if the thresholds for finding markers are changed.

4.3.4 Specifying the marker candidate area in the next frame

The marker candidate area in the next frame is distinguished as 20 pixels of the area which surrounds the marker in the current frame. The bright solar panel surface is located near the markers when GOSAT is in sunshine. Therefore, if the marker candidate area is too large, a light point on the solar panel may be distinguished as a true marker by mistake. The marker candidate area in the next frame is set up as 13 pixels in the upgraded algorithm.

4.4 Examples of image processing results in orbit

Fig. 14 shows enlarged views of the extracted markers, the edges of which are shown here as yellow lines. The paddle and markers are effectively distinguished in all cases of sunshine, penumbra, and umbra.
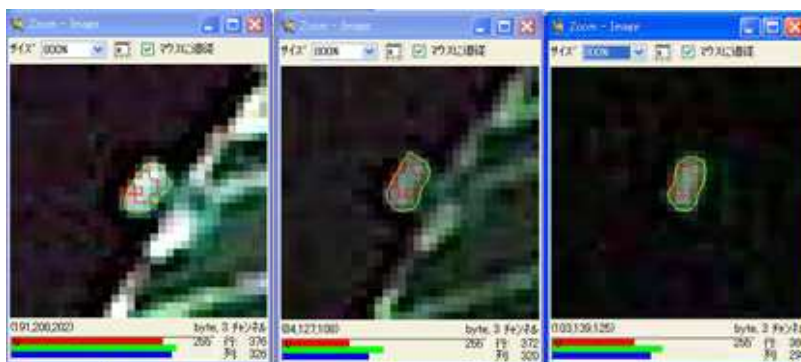
Fig. 14. Results of extracted edges (Left: Sunshine, Centre: Penumbra, Right: Umbra)

5. Measurement and analysis result of vibration using jet thrusters

When a satellite changes its orbit to increase altitude, the installed gas jet thrusters are used, and the solar array panel is subject to deformation or vibration. GOSAT has 20 newton (N) jet thrusters, and a vibration measurement was conducted when they were used. This measurement was conducted to check our measurement system before measuring thermal snap.

5.1 Measurement condition

The measurement of the solar array paddle vibration caused by 20-N thrusters was conducted during the orbital night, for a duration of about 600 seconds. Exposure of the monitoring camera was set to auto, and the resolution of the taken images was set to SXGA (1280 × 1024 pixels).

5.2 Calibration of the external camera parameters

Because the standard calibration table can be set up in the measurement plane, the external camera parameters can be easily obtained in the ground experiment, but not by the method in space. Therefore, the external camera parameters were obtained by using the image of which the GOSAT satellite had taken a photograph while in orbit. The external camera parameter is calculated from the installation position of the camera and the initial marker

and is assumed to be temporary in nature. This temporary external camera parameter is corrected by the image of which the GOSAT satellite took a photograph while in orbit. First, the marker position is obtained in the image coordinate system [Row, Colum] (pixel). Subsequently, two restraint conditions are imposed on the obtained marker position [Row, Column] (pixel). One is that the distance between the markers be constant. Another is that all markers exist in the X-Y plane in the world coordinate system. The external camera parameter is corrected on the restraint condition.

5.3 Evaluation of measurement accuracy based on the distance between two markers

The internal camera parameter was obtained by a prelaunch ground experiment, while the external camera parameter was obtained by the method shown in 5.2. The algorithm shown in 4.2 was used with these parameters for the image processing.

Fig. 15 shows the transition of the distance between markers on the orbit. The average distance between markers was 2393.26 mm, and the standard deviation was 1.99 mm. The design value of the distance between markers of the GOSAT satellite is 2394 ± 2mm. The distance between markers as obtained from the image processing is within this range. The measurement plane is at a position about 5.57 m from the camera, with a resolution of about 7.25 mm/ pixel. Therefore, when the standard deviation is 1.99 mm, the image processing accuracy is about 1/ 3.6 of the resolution.

This accuracy is about 1.5 times compared with the ground experiment result, and has decreased, seemingly due to the darkness of the image. The image darkens when the exposure is set to auto. In the ground experiment, the exposure was set to manual, and the image was processed on the condition that the marker could be subject to clear visual checks. Therefore, the image processing accuracy might improve if the exposure is appropriately set.
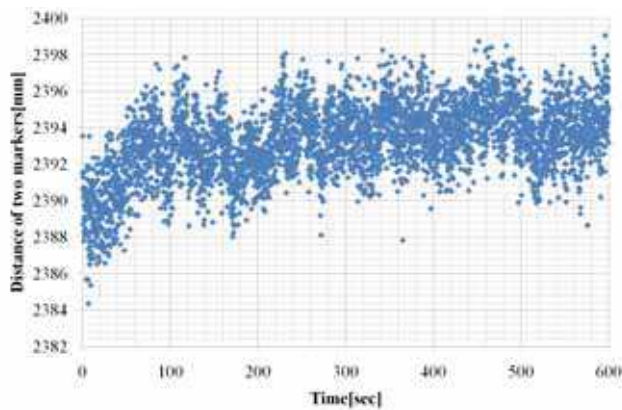

Fig. 15. The transition of the distance between two markers during the 20-N maneuver

5.4 Measurement result of in-plane and out-plane deformations

To evaluate the structural feature of the GOSAT's solar array paddle, vibration analyses are conducted using the result of the image processing conducted when the 20-N thruster was used. Three patterns of the solar array paddle's vibration modes, namely out-of-plane, in-plane, and twist, are considered. The transition of the marker position is written with the

world coordinate system in Fig. 16, meaning the coordinate transformation from the world coordinate system to the local coordinate system of the solar array paddle must be conducted and the transition of the marker must be written with the solar array paddle's local coordinate system to measure the in-plane and out-of-plane vibration which occur on the solar array paddle.

Fig. 17 shows the out-of-plane and in-plane vibration of the marker No. 0. When the 20-N thruster is used, quasi-static deformation is induced while the in-plane and out-of-plane vibration occur. After the 20-N thruster, while the quasi-static deformation reverts, the vibrations continue.

The twist mode of the solar array paddle vibration can be observed based on the transition of the rotation angle of two markers. However, no deformation and vibration are observed from the transition of the rotation angle during the 20-N maneuver.
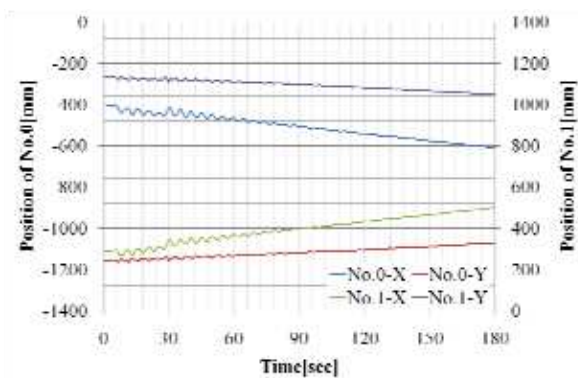
Fig. 16. The transition of the marker position as shown by the world coordinate frame
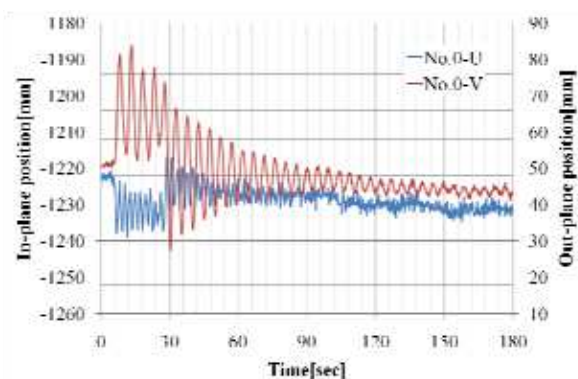
Fig. 17. Measurement result of marker No. 0

5.5 Vibration analysis

Figs. 18 and 19 shows the result of the fast Fourier transform analysis toward the solar array paddle's out-of-plane and in-plane vibration of the maker No. 0's position following the 20-

N thrust. They show that the out-of-plane vibration frequency is 0.215 Hz and the in-plane one is 0.459 Hz. Besides, both markers' in-plane oscillations are in the same phase, meaning no vibration mode, e.g. bending of the solar array panel in the direction of the panel width, occurs.

Based on the results of the fast Fourier transform analyses, 2 patterns of vibration modes can be estimated. Fig. 20 shows the estimated 2 vibration modes of the solar array paddle. The first vibration mode is the first order of the out-of-plane vibration, which is a natural frequency of 0.215 Hz. The second vibration mode is a width direction, which oscillates at 0.459 Hz.
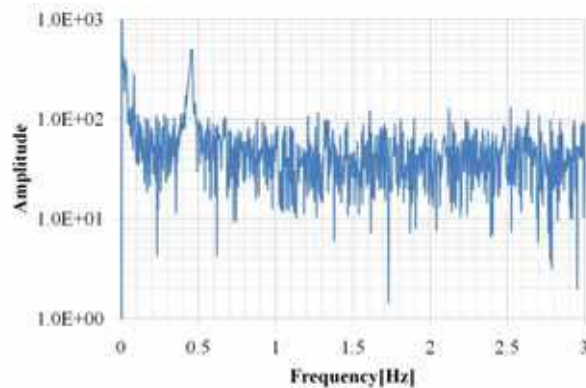
Fig. 18. Result of the FFT analysis (After maneuver, In-plane)
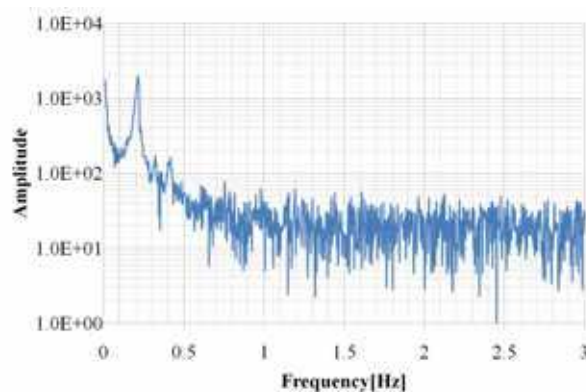
Fig. 19. Result of the FFT analysis (After maneuver, Out-plane)

5.6 Identification of the damping constant

From the out-plane deformation shown in Fig. 17, the damping constant is identified. The twelve peaks after finishing the maneuver are used for the identification. The result of the identification is 0.021, while the damping constant is so small that the natural response frequency of the out-of-plane vibration is very nearly equal to the vibration frequency.
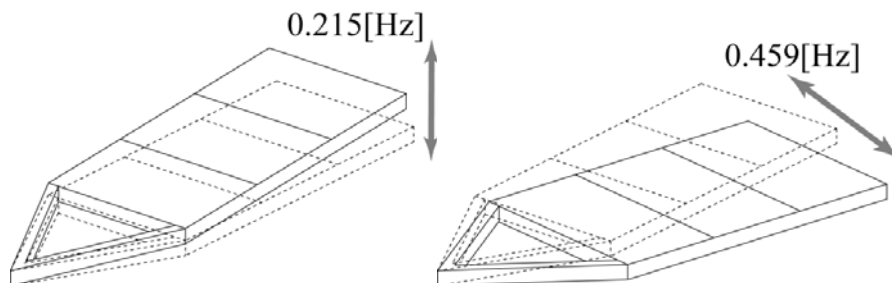
Fig. 20. Estimated vibration mode (Left: 1st. Mode, Right: 2nd. Mode)

6. Measurement result of the thermal snap

The thermally-induced deformation of the solar array paddle is measured when GOSAT goes from the sun side into the shadow of the Earth. To take good images for processing, the appropriate exposure must be set on the monitoring camera and several measurements are conducted as its exposure changes. The images taken at each measurement are subsequently processed to determine the position of the markers based on the adjusted algorithm. The distances between the two markers are evaluated and it is shown that the two markers get close during each measurement, allowing the out-of-plane deformation results of the solar array paddle to be obtained.

6.1 Measurement conditions

Fig. 21 shows the exposure and shooting time, with the LED always on, regardless of the lighting condition and the image resolution SXGA. These conditions are assigned uniform values for all measurements. Images used for measurements are taken when the satellite goes into an eclipse from the sun side. The time is recorded from the point at which the satellite enters the eclipse. The initial 10 seconds is defined as the penumbra, within which the optical environment changes momentarily. The sunshine comes before the penumbra, and the umbra starts 10 seconds after the origin of the latter. The optical environments differ dramatically between the sunshine and eclipse, making it impossible to apply uniform exposure throughout the measurement. If this is done, the brightness of the image taken in the sunshine is saturated, or an image showing nothing is produced when the satellite enters the eclipse. The exposure applied should be varied as appropriate depending on the optical environment. Therefore, several times of measurements are conducted with several exposures and several shooting times. Case 1 shown in Figure 9 is intended to take good images in the umbra, with exposure fixed to 1/ 16, and shooting need not be suspended to change the exposure. Cases 2, 3, and 4 are conducted to take good images in both sunshine and umbra. The optical environment in sunshine is very light, so exposure must be short enough. Exposure is initially set to 1/ 512, 1/ 1024, and 1/ 2048 at first in cases 2, 3, and 4 respectively. After going into the eclipse, the exposures are changed to 1/ 16 to take good images in the umbra in each case.

In cases 5 to 9, measurements start 2 minutes after entering the eclipse, and finish 2 minutes later in terms of elapsed time. Case 5 is conducted as a reference for the other cases, with exposure of 1/ 16. The exposure is set up for the range 1/ 32 to 1/ 256, and fixed in each case.
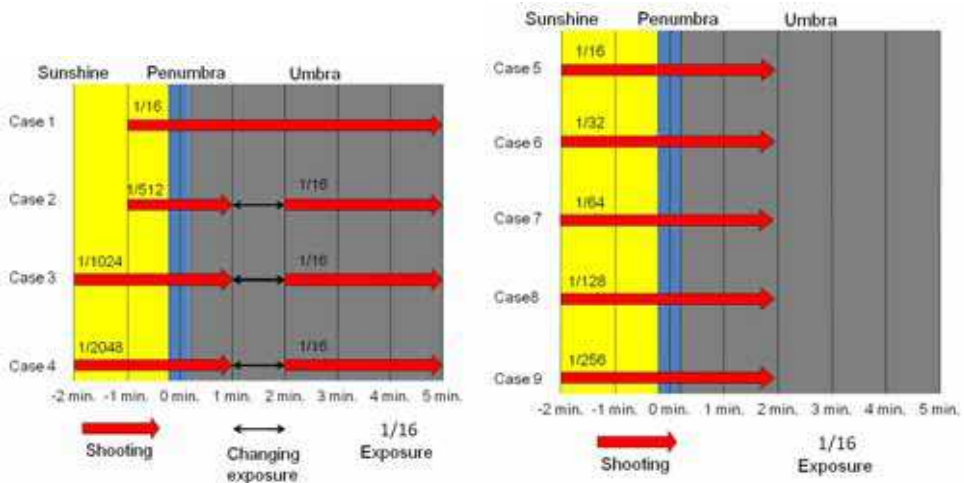
Fig. 21. Measurement condition (Cases 1 ~ 9)

6.2 Result of the thermal snap measurement

Fig. 22 shows examples of images taken in case 1. Fig. 23 is the result of cases 1, 2, 3, and 4, which shows the out-plane displacement of marker No. 0, with the upgraded algorithm for finding markers used to conduct image processing. The orange-colored line shown in Fig. 23, which shows the result of case 1, starts from around the time of origin. Therefore, the image processing succeeds, not only when the satellite is in umbra but also at the end of the penumbra. Rapid deformation occurs in the penumbra, the range of which is about 6 mm. Deformation of the solar array paddle in the umbra starts from about -4.5 mm of the out-plane displacement. Subsequently, the displacement continues to change slowly until about 120 seconds have elapsed from the start of the time elapsed, and then stops. Case 1 shows that rapid deformation occurs at the end of the penumbra, while slow deformation, which is considered quasi-static, occurs after the satellite has completely entered the eclipse. In cases 2, 3, and 4, measurements succeed in both the sunshine and umbra. The image processing is accurate to a sub-pixel level, namely sufficient. When the satellite is in the sunshine, the out-plane displacement of marker No. 0 ranges from about -10 to -7 mm, retaining nearly the same value in each case. Once the satellite enters the eclipse and the exposures are changed, the measurements are conducted again.

The out-plane displacements in the umbra are nearly the same as that of in case 1, but differ when values in the sunshine and umbra are compared. Therefore, the deformation of the solar array paddle is considered to occur from the point the satellite is in the sunshine to that when that is in the umbra.

From cases 1, 2, 3, and 4, displacement in the sunshine and umbra could be respectively obtained. However, displacement in the penumbra could not be measured well due to inappropriate exposure. Fig. 24 shows the results of cases 5, 6, 7, 8, and 9, as well as the out-plane displacement of marker No. 0. Image processing to find markers succeeded from the starting penumbra to the end of measurement in the umbra. The accuracies of each measurement are about plus or minus 1mm, which is sub-pixel level and sufficiently accurate, allowing deformations in the penumbra to be correctly determined. It is shown

that rapid deformation resembling vibration occurs at the solar array paddle of GOSAT while the satellite traverses the penumbra.
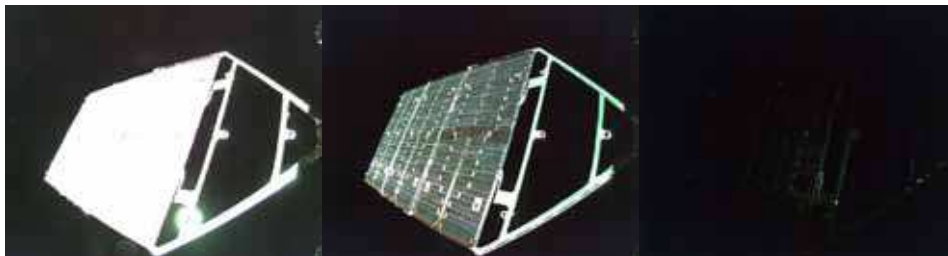

Fig. 22. Examples of images in case 1 (Left: Sunshine, Centre: Penumbra, Right: Umbra)
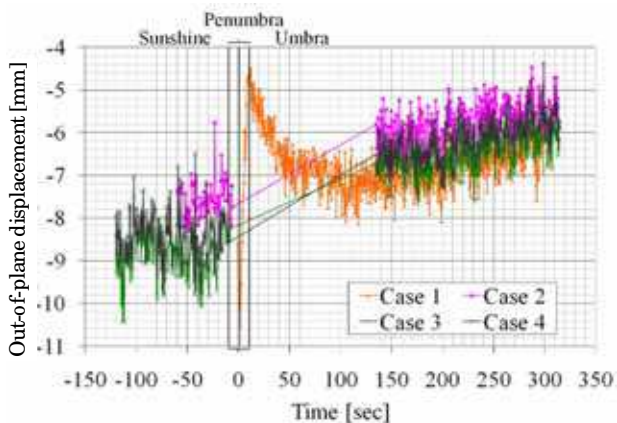

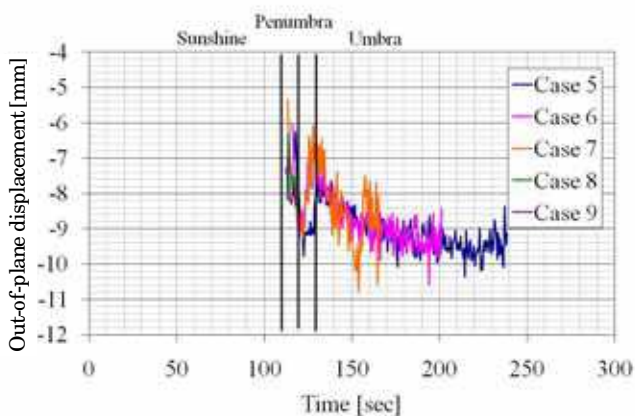Fig. 23. Out-of-plane displacements of marker No. 0 in cases 1, 2, 3, and 4

Fig. 24. Out-of-plane displacement of marker No. 0 in cases 5, 6, 7, 8, and 9

7. Conclusion

In this chapter, a measurement system using an on-board monitoring camera to observe thermal snap in orbit was explained. The thermal snap phenomenon, which causes attitude disturbance of LEO earth observation satellites, has long been observed from gyro telemetry data. However, direct observation of the thermal snap had never succeeded until now. A camera mounted on GOSAT took images when the 20-N thrusters were used and GOSAT went into the eclipse from the sunshine area, and image processing is conducted to measure the displacement of the solar array paddle of GOSAT. To obtain the result around the time of entering the eclipse, the algorithm for extracting the edges of the markers was adjusted by changing the method of detecting the marker candidate area, and the threshold for finding the markers. Based on the measurement during the 20-N maneuver, it was shown that our measurement system could realize sub-pixel measurement accuracy, and the vibration caused by the 20-N maneuver could be observed. Subsequently, the measurements during the transition from sunshine to eclipse showed that deformation of the solar array paddle arose around the time when the satellite went into eclipse.

We are scheduled to conduct additional measurements of the thermal snap phenomena which occur at the solar array paddles of GOSAT because we have not succeeded in conducting an uncut thermal snap measurement from sunshine to umbra.

8. References

Foster, C. L.; Tinker, G. S.; Nurre, W. & Till, W. A. (1995). NASA Technical Paper, *The Solar Array-Induced Disturbance of the Hubble Space Telescope Pointing System,* 3556

Iwata, T.; Hoshino, H.; Yoshizawa, T.; Tanamachi, T.; Kawahara, T. & Gonda, H. (2006). Precision Attitude Determination and Control for the Advanced Land Observing Satellite (ALOS): Flight Results (in Japanese), *Proceedings of the 50th Space Science and Technology Conference,* Japan, 2006

Japan Society of Mechanical Engineering (February 2007). *Mechanical Engineers' Handbook Applications γ11: Space Equipment and Systems,* Japan Society of Mechanical Engineering, ISBN 978-4-88898-154-5, Japan

Johnston, J. D. & Thornton, E. A. (2000). Journal of Spacecraft and Rockets, *Thermally Induced Dynamics of Satellite Solar Panel,* Vol. 37, No. 5 (2000) pp. 604-613

Mobara, M. (October 1994). *Introduction to aerospace engineering –guidance and control of satellite and rocket,* Baifukan, ISBN 978-4-56303-493-1, Japan
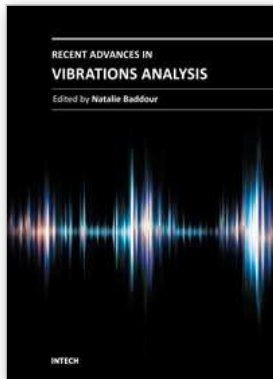
Recent Advances in Vibrations Analysis

Edited by Dr. Natalie Baddour

This book covers recent advances in modern vibrations analysis, from analytical methods to applications of vibrations analysis to condition monitoring. Covered topics include stochastic finite element approaches, wave theories for distributed parameter systems, second other shear deformation theory and applications of phase space to the identifications of nonlinearities and transients. Chapters on novel condition monitoring approaches for reducers, transformers and low earth orbit satellites are included. Additionally, the book includes chapters on modelling and analysis of various complex mechanical systems such as eccentric building systems and the structural modelling of large container ships.

How to reference

In order to correctly reference this scholarly work, feel free to copy and paste the following:

INTECH
open science | open minds